Delta-secretase-cleaved Tau antagonizes TrkB neurotrophic signalings, mediating Alzheimer's disease pathologies

Jie Xiang[a,b], Zhi-Hao Wang[b], Eun Hee Ahn[b], Xia Liu[b], Shan-Ping Yu[c], Fredric P. Manfredsson[d], Ivette M. Sandoval[d], Gong Ju[a], Shengxi Wu[a], and Keqiang Ye[b,1]

[a]Department of Neurobiology, Fourth Military Medical University, Xi'an, 710032 Shaanxi, People's Republic of China; [b]Department of Pathology and Laboratory Medicine, Emory University School of Medicine, Atlanta, GA 30322; [c]Department of Anesthesiology, Emory University School of Medicine, Atlanta, GA 30322; and [d]Department of Translational Science & Molecular Medicine, Michigan State University, Grand Rapids, MI 49503

Edited by Solomon H. Snyder, Johns Hopkins University School of Medicine, Baltimore, MD, and approved March 28, 2019 (received for review January 26, 2019)

BDNF, an essential trophic factor implicated in synaptic plasticity and neuronal survival, is reduced in Alzheimer's disease (AD). BDNF deficiency's association with Tau pathology in AD is well documented. However, the molecular mechanisms accounting for these events remain incompletely understood. Here we show that BDNF deprivation triggers Tau proteolytic cleavage by activating δ-secretase [i.e., asparagine endopeptidase (AEP)], and the resultant Tau N368 fragment binds TrkB receptors and blocks its neurotrophic signals, inducing neuronal cell death. Knockout of BDNF or TrkB receptors provokes δ-secretase activation via reducing T322 phosphorylation by Akt and subsequent Tau N368 cleavage, inducing AD-like pathology and cognitive dysfunction, which can be restored by expression of uncleavable Tau N255A/N368A mutant. Blocking the Tau N368–TrkB complex using Tau repeat-domain 1 peptide reverses this pathology. Thus, our findings support that BDNF reduction mediates Tau pathology via activating δ-secretase in AD.

AEP | Tau N368 | BDNF deprivation | Tauopathy | Alzheimer's disease

Alzheimer's disease (AD), the most common form of dementia, is a progressive neurodegenerative disease characterized by the extracellular accumulation of amyloid-β peptide (Aβ) and the intraneuronal aggregation of neurofibrillary tangles (NFTs) composed of truncated and hyperphosphorylated Tau. Emerging evidence suggests that BDNF may be important for the pathogenesis of AD. BDNF, a secreted protein, is a member of the neurotrophins, along with NGF and neurotrophins 3 and 4/5. BDNF regulates neuronal survival, differentiation, and plasticity by activating the receptor tyrosine kinase TrkB and p75 low-affinity neurotrophin receptor (1). BDNF binding to its high-affinity receptor, TrkB, triggers Ras/Raf/MAPK, PI3K/Akt, and PLC-γ1 signal activation and is essential for the induction and maintenance of long-term potentiation (LTP) and for long-term memory (2). BDNF and TrkB expression levels are reduced in postmortem brains of AD patients (3–5). Further, BDNF levels are decreased at the mild cognitive impairment stage of the disease and correlate with cognitive function (6). A significant decrease in BDNF mRNA and protein levels in non-AD tauopathies have been reported (7). Moreover, accumulating data suggest that BDNF polymorphisms are associated with an increased risk of developing AD (8). Interestingly, neurons containing NFT do not contain BDNF immunoreactivity, whereas neurons with a high degree of BDNF are devoid of tangles (9). Hence, these studies suggest that BDNF may have a protective role against AD pathogenesis. Accordingly, BDNF displays protective effects on neuronal toxicity induced by Aβ peptides in vitro and in vivo (10, 11). BDNF coincubation in hippocampal (12) or entorhinal cortical slices (13) also prevents Aβ42-induced impairment in LTP induction. In P301S mouse retinal ganglion cells, the impairment of TrkB signaling is triggered by Tau pathology and mediates the Tau-induced dysfunction of visual response (14). The beneficial effect of BDNF administration has been shown to increase learning and memory of demented animals (15). Decreased BDNF levels are associated with synaptic and neuronal loss and cognitive impairment with aging and AD, but there is little evidence showing that BDNF signaling would play a major role in the disease-specific amyloid or Tau pathology.

Mammalian asparagine endopeptidase (AEP; also called δ-secretase, *LGMN*) is an age-dependent protease (16). It is mainly regulated by posttranslational modification including caspase-3 cleavage at N-terminal D25 and autocleavage at N323, yielding a fully active and mature 36-kDa form (17, 18). AEP is a lysosomal enzyme, and its activation is predominantly mediated by acidosis. Previously, we reported that AEP is activated during stroke and subsequently cleaves SET, a DNase inhibitor and PP2A inhibitor, mediating neuronal cell death (18). Recently, we have reported that AEP is activated in AD mouse brains and AD patient brains, and it cleaves Tau at N255 and N368 residues and abolishes its microtubule binding activity, promoting its aggregation and neurotoxicity (16). Moreover, we have showed that AEP also acts as a δ-secretase that cleaves APP at N373 and N585 residues in the endolysosome, yielding an efficient substrate APP (C586–695) fragment that allows BACE1 to prominently generate Aβ (19). KO of AEP from Tau P301S or 5XFAD mice substantially reduces the tauopathies or amyloid plaque pathologies, rescuing the cognitive functions in these transgenic AD mouse models. On the contrary, inhibition of AEP with small-molecule inhibitors results in pronounced therapeutic efficacy in

Significance

BDNF is important in neuronal survival and synaptic plasticity. BDNF level reduction in Alzheimer's disease (AD) is well documented, but it remains unclear whether BDNF deficiency contributes to AD pathology. We show that BDNF deprivation provokes asparagine endopeptidase (AEP) activation via reducing δ-secretase (AEP) T322 phosphorylation by Akt and subsequently cleaves Tau at N368 residue and enhances its binding with TrkB receptors, blocking the neurotrophic signals. Our data demonstrate that AEP-cleaved Tau N368 interacting with TrkB might account for BDNF reduction-triggered AD pathologies.

Author contributions: J.X. and K.Y. designed research; J.X., Z.-H.W., E.H.A., X.L., F.P.M., and I.M.S. performed research; J.X., S.-P.Y., G.J., S.W., and K.Y. analyzed data; and J.X. and K.Y. wrote the paper.

The authors declare no conflict of interest.

This article is a PNAS Direct Submission.

[1]To whom correspondence should be addressed. Email: kye@emory.edu.

This article contains supporting information online at www.pnas.org/lookup/suppl/doi:10.1073/pnas.1901348116/-/DCSupplemental.

Published online April 17, 2019.

various AD mouse models (20). In addition to Tau and APP, we found that AEP also cleaves α-synuclein at N103 and enhances its aggregation and neurotoxicity, promoting Parkinson's disease pathology (21). Interestingly, we reported that serine-arginine protein kinase 2 (SRPK2) phosphorylates serine 226 on AEP in AD and accelerates its autocatalytic cleavage, leading to its cytoplasmic translocation and elevated enzymatic activity (22). Most recently, we demonstrated that BDNF/TrkB-activated Akt phosphorylates δ-secretase on T322, inhibiting its maturation and activation. T322-phosphorylated δ-secretase is sequestered in the lysosomes (23). Together, these studies support that δ-secretase plays a pivotal role in the pathogenesis of neurodegenerative diseases including AD, mediating the cognitive dysfunctions during the aging process.

Accumulating evidence demonstrates that Tau overexpression or hyperphosphorylation down-regulates BDNF expression in primary neurons and AD animal models (24, 25). On the contrary, BDNF also mediates Tau expression, phosphorylation, and subcellular distribution that may be implicated in neuronal morphological plasticity (26, 27). The toxic gain of function associated with Tau aggregates and loss of its normal physiological microtubule dynamics are thought to mediate the toxicity of NFT. However, the exact molecular mechanisms of how Tau N368 exerts its detrimental effects remain unclear. In the present study, we show that BDNF depletion inhibits δ-secretase T322 phosphorylation by Akt and induces its activation that subsequently cleaves Tau N368, which, in turn, binds the TrkB receptor on its C terminus and antagonizes neurotrophic signaling, triggering neuronal apoptosis. Preventing Tau cleavage by δ-secretase or blocking Tau N368/TrkB association in BDNF-depleted mice rescues neurotrophic signaling and represses neuronal apoptosis, up-regulating synaptic plasticity and learning and memory.

Materials and Methods

Mice, Primary Cultured Neurons, Cell Lines, and Human Tissue Samples. WT C57BL/6J 000664, BDNF2lox 004339, P301S 008169, and 3xTg 34380 mice were ordered from the Jackson Laboratory (cat. nos. 000664, 004339, 008169, and 34830, respectively). Animal care and handling was performed according to National Institutes of Health animal care guidelines and Emory Medical School guidelines. The protocol was reviewed and approved by the Emory University Institutional Animal Care and Use Committee. Primary rat cortical neurons were cultured as previously described (16). All rats were obtained from the Jackson Laboratory. HEK293 was cultured in high-glucose DMEM with 10% FBS and penicillin (100 U/mL)/streptomycin (100 mg/mL; all from HyClone). SH-SY5Y and SH-SY5Y (TrkB, BR6) cells were cultured in DMEM/F12 supplemented with 10% FBS, penicillin (100 U/mL), and streptomycin (100 μg/mL; all from HyClone). Cells were incubated at 37 °C in a humidified atmosphere of 5% CO_2. Postmortem brain samples were dissected from frozen brains of AD and age-matched nondemented controls from the Emory University Alzheimer's Disease Research Center. The study was approved by the Institutional Animal Care and Use Committee (IACUC) at Emory University. AD was diagnosed according to the criteria of the Consortium to Establish a Registry for AD and the National Institute on Aging. Diagnoses were confirmed by the presence of amyloid plaques and NFTs in formalin-fixed tissue. Informed consent was obtained from the subjects.

Transfection and Infection of Cells. HEK293 transfection was performed with Lipofectamine 2000 (Invitrogen). SH-SY5Y transfection was performed by using Lipofectamine 3000 (Invitrogen). AAV-Cre and AAV-GFP used in neuronal cultures were packaged in the Emory University Viral Vector Core with a titer of 1×10^{13} genome copies (GC)/mL and 7×10^{12} GC/mL, respectively. To express AAV-Cre virus in $BDNF^{2lox}$ mouse primary neurons to eliminate BDNF, 3 μL AAV-Cre virus was added to 1 mL culture medium. To express Tau N368 in primary neurons, 0.2 μL, 0.5 μL, or 1.0 μL AAV-Tau N368 was added to 1 mL culture medium. AAV-Tau N368 and AAV-Tau N255A/N368A combined with human Synapsin I gene promoter were packaged by the laboratory of F.P.M. at Michigan State University. The viral titer was $1–5 \times 10^{13}$ GC/mL.

BDNF Withdrawal Experiment. BDNF withdrawal experiments were performed as previously described (28). Primary cortical neurons were isolated from day 16–17 pregnant C57BL6 mice. Following 2 d culture in neurobasal medium with B-27 supplement and GlutaMAX, cytosine arabinofuranoside was added to decrease glial proliferation. Neurons were exposed to BDNF (50 ng/mL, 450–02; PeproTech) for 48 h at 3–4 d after plating, and subsequently the medium was rinsed three times with neurotrophin-free medium and then incubated for another 48 h in the same medium containing BDNF mAb (30 μg/mL, NBP2-42215; Novus) or the same concentration of mouse IgG2a kappa (14–4724-82; Invitrogen). Then, cell lysates were prepared for immunoblotting or coated slices were fixed for immunofluorescent staining.

AEP Activity Assay. AEP activity assay was performed as previously described (23). Tissue homogenates or cell lysates (10 μg) were prepared and incubated with 200 μL reaction buffer (60 mM Na_2HPO_4, 20 mM citric acid, 1 mM EDTA, 0.1% CHAPS, and 1 mM DTT, pH 5.5) containing 20 μM AEP substrate Z-Ala-Ala-Asn-AMC (Bachem). AMC released by substrate cleavage was quantified at 460 nm in a fluorescence plate reader at 37 °C in kinetic mode.

Immunoprecipitation and Western Blot Analysis. Cells were washed in PBS solution and lysed in coimmunoprecipitation (co-IP) buffer (50 mM Tris·HCl, pH 7.5, 150 mM NaCl, 1% Nonidet P-40, 5 mM EDTA, 5 mM EGTA, 15 mM $MgCl_2$, 60 mM β-glycerophosphate, 0.1 mM sodium orthovanadate, 0.1 mM NaF, 0.1 mM benzamide, 10 mg/mL aprotinin, 10 mg/mL leupeptin, and 1 mM PMSF) at 4 °C (23). Immunoprecipitated proteins were separated by SDS/PAGE and then transferred to a nitrocellulose membrane. The transferred membrane was blocked with Tris-buffered saline (TBS) solution containing 5% nonfat milk and 0.2% Tween 20 (TBST) at room temperature (RT) for 1 h, followed by overnight primary antibody incubation at 4 °C and with the secondary antibody at RT for 2 h. After washing with TBST three times, the membrane was developed by using the Enhanced Chemiluminescent detection system. Rabbit anti-Tau N368 antibody (0.25 mg/mL; laboratory of K.Y.) was used in co-IP at 1:1,000 and 1:2,500 in mouse brain Western blot (WB), 1:4,000 in patient brain WB, and 1:1,000 in primary rat cortical neuron.

GST-Pull Down. GST pull-down was described previously (23) with steps as follows. Add the clarified cell lysate into 50 μL 50% slurry of glutathione–Sepharose 4B with immobilized GST/GST fusion protein for 2–4 h at 4 °C with end-over-end mixing. Sediment the medium by centrifugation at $500 \times g$ for 5 min. Carefully decant the supernatant. Wash the glutathione–Sepharose 4B by adding 1 mL lysate buffer to each tube. Invert to mix. Elute the interacting protein complex by centrifugation at $500 \times g$ for 5 min. Carefully decant the supernatant. Repeat three times and collect the sediment for further processing.

Immunohistochemistry. Immunohistochemistry was performed by using the peroxidase protocol (23). Briefly, tissue sections were rehydrated in xylene and hydrated through descending ethanol, and slides were brought to a boil in 10 mM sodium citrate buffer, pH 6.0, for antigen retrieval up to 30 min. Sections were washed in distilled water three times. Endogenous peroxidase activity was quenched by incubation in 3% hydrogen peroxide for 10 min. Then, each section was blocked with 100–400 μL blocking solution for 1 h at RT in a humidified chamber. The sections were incubated with primary antibodies overnight at 4 °C. The signal was developed by using a Histostain-SP kit (Invitrogen). For double immunofluorescence staining, the sections were incubated overnight at 4 °C with a mixture of antibodies. After being washed with TBS solution, the sections were incubated with a mixture of Alexa Fluor 488- and 568-coupled secondary antibodies (Invitrogen) for detection. Images were acquired with confocal imaging (FV1000; Olympus). Anti-Tau N368 (0.25 mg/mL; laboratory of K.Y.) was used at 1:500.

Administration of Tat–Repeat-Domain 1–FITC. Mice were i.p. administered 10 mg/kg Tat–repeat-domain 1 (R1)–FITC (GRKKRRQRRRPQQTAPVPMPDLKNVKSKIGSTENLKHQPGGGK) or Tat–scrambled R1 (sR1)–FITC as control (GRKKRRQRRRPQDSVLKKNAMKKTLPTNGHSPEQVIPGGPQGK) once every 5 d consecutively for 6 wk, 7 d after injection of AAV-Cre virus at hippocampal CA1 region. To test whether the Tat peptide could be delivered into the brain, Tat-R1-fluorescein (i.e., FITC, 10 mg/kg, i.v.) was injected. At 1, 3, 5, and 7 d after injection, brain sections (30 μm) were imaged with a confocal microscope. Peptides with 98% purity were synthesized by Peptide 2.0.

Aβ Plaque Staining. Thioflavin-S was used to detect fibrillar Aβ plaque deposition. Sections were deparaffinized and allowed to dry. The sections were incubated for 5 min with 0.0125% Thioflavin-S in 50% ethanol. The sections were washed with 50% ethanol and placed in distilled water. Then, the sections were covered with a glass cover with use of mounting solution. Quantitative assessment of plaque areas was counted by using ImageJ

software. Five sections per animal were counted. Slides were imaged by using an FV1000 fluorescence microscope (Olympus).

Transmission EM. Synapse quantification was performed by using transmission EM as described previously (29). After deep anesthesia was achieved, mice were perfused transcardially with 2% glutaraldehyde and 3% paraformaldehyde in PBS solution. Tissue blocks were embedded, and 90-nm sections were cut by ultramicrotome. The sections were stained with uranyl acetate followed by lead acetate and examined at 100 kV in a 200CX electron microscope (JEOL). Synapses were identified by the presence of synaptic vesicles and postsynaptic densities.

Stereotaxic Injection of AAV in Mouse CA1. $BDNF^{2lox}$ mice aged 3–4 mo and weighing ∼35 g received bilateral injections as described previously (23). Briefly, animals were anesthetized with i.p. injections of 100/10 mg/kg ketamine/xylazine and given 0.1 mg/kg buprenorphine s.c. for pain management. Depth of anesthesia was assessed via toe pinch. Stereotaxic hippocampal CA1 region coordinates were (from bregma) anteroposterior, −2.2 mm; mediolateral, ±1.7 mm; and dorsoventral, 1.6 mm. Injection rate was 0.2 μL/min at doses ranging from 0.5 to 1×10^{13} GC/mL for a total of 5 min per injection, with the needle left in place for 1 min postinjection. After injections, the incision was sutured and triple antibiotic ointment was applied. Animals recovered on heating pads until awake and were monitored 1, 2, 7, and 10 d postsurgery. All surgeries were performed with approval from the IACUC at Emory University. Mice were assigned to sex- and age-matched treatment groups by using a randomized block design.

Golgi Staining. Mouse brains were fixed in 10% formalin for 24 h and then immersed in 3% potassium bichromate for 3 d in the dark. The solution was changed every day. Brains were then immersed in 2% silver nitrate solution for 2–3 d in the dark. Vibratome sections were cut approximately 20–30 μm in thickness, air-dried for 10 min, dehydrated in ethanol, cleared, and mounted.

Electrophysiology. Acute hippocampal transversal slices were prepared from different ages of $BDNF^{2lox}$ and WT mice treated with the various AAV vectors or peptides as previously described (16, 19). Briefly, mice were anesthetized with isoflurane and decapitated, and brains were immersed in ice-cold artificial cerebrospinal fluid (a-CSF) containing 124 mM NaCl, 3 mM KCl, 1.25 mM NaH_2PO_4, 6.0 mM $MgCl_2$, 26 mM $NaHCO_3$, 2.0 mM $CaCl_2$, and 10 mM glucose. Hippocampi were dissected and sliced into 400-μm-thick transverse slices with a vibratome. After incubation at RT (23–24 °C) in a-CSF for 60–90 min, slices were placed in a recording chamber (RC-22C; Warner Instruments) on the stage of an upright microscope (CX-31; Olympus) and perfused at a rate of 3 mL/min with a-CSF (containing 1 mM $MgCl_2$). A 0.1-MU tungsten monopolar electrode was used to stimulate the Schaffer collaterals. A glass microelectrode filled with a-CSF with resistance of 3–4 MU was placed to measure field excitatory postsynaptic potentials (fEPSPs) in CA1 stratum radiatum. The stimulation output (Master-8; AMPI) was controlled by the trigger function of an EPC9 amplifier (HEKA Elektronik). fEPSPs were recorded under current-clamp mode. Data were filtered at 3 kHz and digitized at sampling rates of 20 kHz using Pulse software (HEKA Elektronik). The stimulus intensity (0.1-ms duration, 10–30 mA) was adjusted to evoke 40% of the maximum fEPSP, and the test pulse was applied at a rate of 0.033 Hz. LTP of fEPSPs was induced by three theta-burst stimulations (four pulses at 100 Hz repeated three times with a 200-ms interval). The magnitudes of LTP are expressed as the mean percentage of baseline fEPSP initial slope.

Morris Water Maze. Different ages of $BDNF^{2lox}$ and WT mice treated with the various AAV viruses or peptides were trained in a round, water-filled tub (52-in diameter) in an environment rich with extramaze cues as described previously (16). Each subject was given four trials daily for five consecutive days with a 15-min intertrial interval. The maximum trial length was 60 s, and if subjects did not reach the platform in the allotted time, they were manually guided to it. Following the 5 d of task acquisition, a probe trial was presented, during which time the platform was removed and the percentage of time spent in the quadrant that previously contained the escape platform during task acquisition was measured over 60 s. All trials were analyzed for latency and swim speed by means of MazeScan (Clever Sys).

Contextual Fear Conditioning. As described previously (16), mice were placed in operant chambers (7″ W, 7″ D, 12″ H; Coulbourn) composed of Plexiglass with a metal shock grid floor, and mice (n = 10 per genotype) were trained and tested on three consecutive days. Every day, mice explored the enclosure for 3 min. Following this habituation period, three conditioned stimulus (CS)–unconditioned stimulus (US) pairings were presented with a 1-min intertrial interval. The CS was composed of a 20-s, 85-dB tone, and US was composed of 2 s of a 0.5-mA foot shock, which was simultaneous with each CS presentation. One minute following the last CS–US presentation, mice were returned to their home cage. Twenty-four hours after the training, mice were returned to the same chambers and presented with a context test. The amount of freezing was recorded via a camera and the software provided by Coulbourn. No shocks were given during the context test. On day 3, a tone test was presented, during which time subjects were exposed to the CS in a novel compartment. Initially, animals were explored in the novel context for 2 min. Then, the 85-db tone was presented for 6 min and the amount of freezing behavior was measured.

Novel Object Recognition. The novel object recognition test was modified from a previously described method (30). Spatial memory was measured in a white plastic chamber (28 × 28 cm). The apparatus was unscented, and intermediate lighting was used. All mice were transferred to the behavioral room 30 min before the training session to familiarize them with the environment. On day 1, mice were allowed to freely explore the chamber with patterns for 15 min. On day 2, mice were introduced into the chamber with an object (7-cm-tall glass flask filled with metal beads) placed adjacent to either patterned wall. The position of the object was counterbalanced within each genotype. On day 3, mice were placed into the chamber with the object in the same position as the previous exposure (i.e., familiar) or at a novel location based on wall patterning. The time spent exploring each object until 20 s of total exploration time was reached was recorded on a stopwatch. Total time exploring the object was also measured (nose within 1.5 cm of object; up to 10 min). Raw data were extracted and analyzed by using Excel (Microsoft). Preference index was calculated as $(T_N - T_F)/(T_N + T_F)$, with T_N as time for novel object and T_F as time for familiar object.

Quantification and Statistical Analysis

All data are expressed as mean ± SEM from three or more independent experiments, and the level of significance between two groups was assessed with Student's t test. For more than two groups, one-way ANOVA followed by least significant difference post hoc test was applied. A value of $P < 0.05$ was considered to be statistically significant.

Results

δ-Secretase–Cleaved Tau N368 Selectively Interacts with TrkB Receptors. BDNF and Tau mutually affect each other's expression (14, 24, 26). However, it remains unclear whether these effects are directly linked. To explore the molecular relationship between Tau and Trk receptors, we cotransfected mammalian GST-tagged Tau (mGST) and HA-Trk plasmids into HEK293 cells. GST pull-down indicated that Tau selectively interacted with TrkB, but not TrkA or TrkC (Fig. 1*A*). To assess the effect of BDNF in this event, we conducted the binding assay in TrkB receptor stably transfected SH-SY5Y cells (called BR6). It is worth noting that truncated Tau N368 displayed stronger binding activity to TrkB than full-length (FL) Tau in the absence of BDNF. Notably, BDNF treatment reduced the interaction by FL Tau and Tau N368 with TrkB, whereas Tau N368 associated with TrkB more robustly (Fig. 1*B*). Co-IP studies using a Tau N368 antibody with brain lysates revealed that endogenous Tau N368 selectively bound to TrkB with much stronger activity in Tau P301S mice than in WT mice. In alignment with this finding, there is abundant Tau N368 truncation in Tau P301S but not WT mice (Fig. 1*C*). We made similar observations in human AD brains vs. healthy controls. As expected, p-TrkB signalings were reduced in AD brains. AEP was highly activated in AD brains, correlating with demonstrable presence of Tau N368, fitting with its tighter association with TrkB in AD brains than controls (Fig. 1*D*). Immunofluorescent costaining demonstrated that Tau N368 signals were elevated upon BDNF withdrawal, colocalizing with total TrkB in primary hippocampal neurons. On the contrary, p-TrkB Y816 was decreased with increased concentration of Tau N368 in the soma of primary neurons (Fig. 1*E*). Mapping assays showed that the C-terminal tail on TrkB, where PLC-γ1 interacts, was implicated in binding of Tau via its repeat

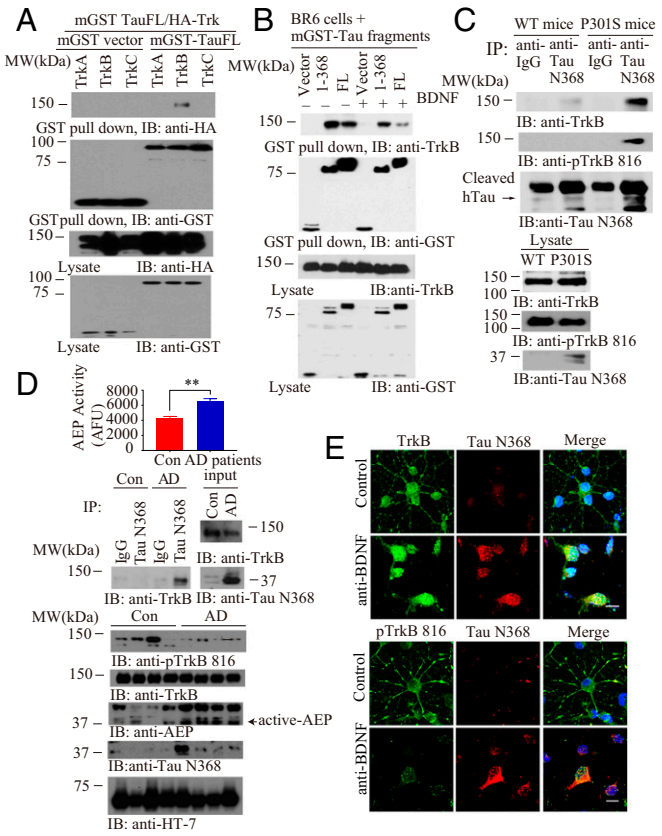

Fig. 1. δ-Secretase–cleaved Tau N368 selectively interacts with the TrkB receptors. (*A*) Tau specifically interacts with the TrkB receptors. GST pull-down assay was conducted from HEK293 cells. (*B*) BDNF mediates Tau/TrkB association. BR6 cells transfected with mGST-Tau FL or Tau N368 followed by BDNF treatment (50 ng/mL) for 15 min. (*C*) Tau N368 associates with TrkB in P301S mice brains. Brain lysates from WT and P301S mice were immunoprecipitated with anti-Tau N368 before immunoblotting with anti-TrkB and anti–p-TrkB 816. (*D*) Tau N368 interacts with the TrkB receptors and reduces TrkB signaling in AD human patient brains. AEP activity assay (*Top*). (Mean ± SEM of five samples per group; $^{**}P < 0.01$.) Brain lysates from AD patients or controls were immunoprecipitated with anti-Tau N368 before immunoblotting with anti-TrkB (*Middle*). Brain lysates were probed with various antibodies (*Bottom*). (*E*) TrkB and p-TrkB 816 colocalize with Tau N368 in BDNF-withdrawal primary cortical neurons. Primary cortical neurons were treated with anti-IgG or anti-BDNF 15 μg/mL for 48 h, and immunofluorescent costaining was conducted. (Scale bar, 10 μm.)

domains (RDs; amino acids 256–368). Noticeably, the RD regions aggregated into oligomers with molecular weights of ∼60 and 75 kDa (size of GST-tagged monomer is 37 kDa; *SI Appendix*, Fig. S1 *A–C*). The amino acid number is based on the longest Tau isoform (isoform 2, amino acids 1–441). To avoid confusion, we adopted isoform 2's numbering system even though we employed isoform 4 (1–352) in our in vitro experiments. A competition assay showed that the R1 domain, but not the R3 or R4 domains, entirely disrupted the association between Tau N368 and TrkB (*SI Appendix*, Fig. S1*D*), suggesting that the R1 domain on Tau binds to the TrkB C-terminal tail. Noticeably, kinase-dead TrkB displayed weaker binding affinity to Tau N368 than TrkB WT (*SI Appendix*, Fig. S1*E*), indicating that the tyrosine kinase activity on TrkB receptors somehow mediates the association between Tau and TrkB. δ-Secretase increases with age in the mouse brain, as does Tau N368 (16). Accordingly, we monitored p-TrkB Y816 signals in different ages of WT, Tau P301S, and 3xTg mice. Interestingly, p-TrkB activity was reduced in an age-dependent manner in Tau P301S and 3xTg mice and completely suppressed in 13-mo-old cohorts of these mice. Moreover, δ-secretase was activated in these mice, correlating with Tau N368 levels (*SI Appendix*, Fig. S1 *F* and *G*).

Tau N368 Inhibits TrkB Neurotrophic Signaling Pathways and Induces Neuronal Cell Death. To investigate the effect of Tau N368 association on TrkB neurotrophic signaling pathways, we treated BR6 cells transfected with Tau N368 with BDNF. p-TrkB Y816 was completely blocked by Tau N368 in the absence of BDNF compared with control. Overexpression of Tau N368 suppressed BDNF-triggered TrkB phosphorylation and downstream p-Akt and p-MAPK. The interaction between TrkB and Tau N368 was slightly reduced in the presence of BDNF (Fig. 2*A*). To examine the association between Tau N368 and TrkB on BDNF neurotrophic signaling in neurons, we treated primary neuronal cultures with anti-BDNF or control antibody. The BDNF antibody triggered Tau N368 production in the neurons, coupled with demonstrable δ-secretase activation (Fig. 2*C*). In alignment with these findings, p-TrkB and its downstream effectors p-Akt and p-MAPK were reduced in the presence of anti-BDNF. Moreover, an association between Tau N368 and TrkB was detected when BDNF was withdrawn (Fig. 2*B*). To further test the effect of Tau N368 on TrkB signaling, we infected primary cultures with various amounts of virus expressing Tau N368 and found that a progressive increase in Tau N368 gradually repressed TrkB Y816 and Y706 phosphorylation, with the associated downstream changes in p-Akt and p-MAPK. Importantly, active caspase-3 was steadily increased, corresponding with the increase in Tau N368 (Fig. 2*D*), indicating that Tau N368 overexpression inhibits TrkB neurotrophic pathways and induces neuronal apoptosis. To evaluate whether BDNF deprivation-induced neurotrophic signaling reduction and apoptosis is mediated by Tau N368 production, we treated the primary neuronal cultures with BDNF withdrawal in the presence of anti-Tau N368 or control IgG. BDNF deprivation induced a reduction in TrkB Y816 phosphorylation that was dose-dependently restored by anti-Tau N368 (as was Akt and MAPK phosphorylation). In accordance with the recovery of TrkB-mediated neurotrophic signaling, BDNF withdrawal-elicited apoptosis was inhibited in the same fashion, and closely coupled with Tau N368 levels in the neurons (Fig. 2*E*). BDNF deprivation resulted in detectable Tau N368 and Aβ42 in the neuronal medium (*SI Appendix*, Fig. S2 *A* and *B*). Moreover, the lactate dehydrogenase (LDH) assay supported that BDNF withdrawal-incurred neuronal cell death was significantly blocked by Tau N368 antibody in a dose-dependent manner (Fig. 2*F*). Employing δ-secretase–null primary neurons, we found that BDNF deprivation resulted in reduced apoptosis compared with WT neurons, in alignment with the abundance of Tau N368 (*SI Appendix*, Fig. S2*C*). Again, these observations were also validated by LDH assay (*SI Appendix*, Fig. S2*D*). Together, these data support that anti-BDNF–induced Tau N368 plays an important role in BDNF withdrawal-triggered repression in TrkB signaling and the resultant neuronal cell death.

Depletion of BDNF or TrkB Activates δ-Secretase via Inhibiting Akt Phosphorylation on T322. Recently, we showed that Akt phosphorylates δ-secretase on T322 residue and sequesters it into the lysosomes, repressing its enzymatic activation (23). To explore whether this action is implicated in δ-secretase activation as a result of the blockade of BDNF/TrkB signaling, we prepared primary neuronal cultures from $BDNF^{2lox}$ mice and knocked out BDNF by infecting neurons with Cre virus or control virus. Immunoblotting showed that depletion of BDNF evidently inhibited p-TrkB Y816 activation, resulting in p-Akt suppression. Accordingly, p-δ-secretase T322 was eradicated in neurons without BDNF (Fig. 3*A*). As expected, δ-secretase enzymatic activities were significantly enhanced when BDNF was depleted (Fig. 3*B*). To interrogate the role of BDNF/TrkB pathway in regulating δ-secretase activity, we knocked out TrkB receptors in

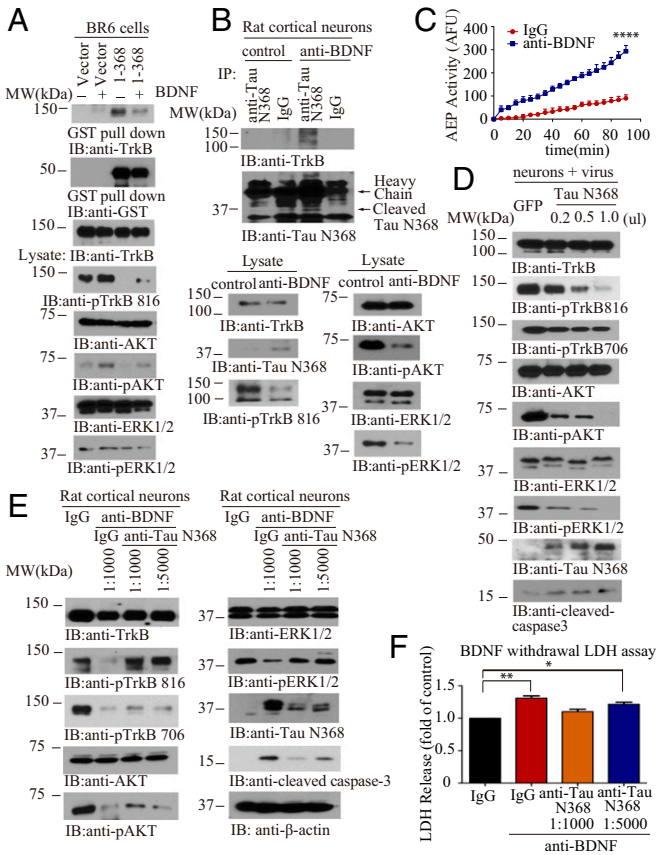

Fig. 2. Tau N368 suppresses BDNF-TrkB signaling. (*A*) BDNF reduces the association between Tau N368 and TrkB. The binding between Tau N368 and TrkB was confirmed using GST pull-down. (Top three panels) p-TrkB and its downstream effectors were analyzed in the cell lysates. (*B*) Tau N368 associates with TrkB receptors in anti-BDNF–treated primary cortical neurons. Immunoprecipitation with anti-Tau N368 and immunoblotting with anti-TrkB (*Top* and *Middle*). Western blot analysis of TrkB signaling and AEP cleavage of Tau N368 (*Bottom*). (*C*) Validation of AEP enzymatic activities by fluorescent substrate cleavage assay. (Data represent mean ± SEM of three independent experiments; $^{****}P < 0.0001$.) (*D*) Tau N368 dose-dependently represses TrkB signaling and apoptosis. Primary cortical neurons were infected with different amount of AAV-Tau N368 virus or GFP control. Immunoblotting analysis was performed by using cell lysates. (*E* and *F*) BDNF withdrawal-induced TrkB signaling reduction and neural cell death are mediated by Tau N368 production. Primary cortical neurons were treated with 30 μg/mL anti-BDNF in the presence of anti-Tau N368 (0.25 mg/mL) with different dilutions for 48 h, and immunoblotting analysis of cell lysates with various antibodies (*E*) and LDH assay were conducted with cell medium (*F*). (Data represent mean ± SEM of three independent experiments; $^{*}P < 0.05$ and $^{**}P < 0.01$.)

TrkB f/f primary neurons with Cre virus, followed by BDNF stimulation for different times. In control neurons, BDNF temporally activated TrkB and its downstream effector Akt. By contrast, these events were totally diminished when TrkB receptors were knocked out. Consequently, p-δ-secretase T322 was decreased, which was associated with robust truncation and maturation of δ-secretase (Fig. 3*C*, sixth panel from the top). Accordingly, APP and Tau were robustly truncated at N585 and N368 by active δ-secretase, respectively. Notably, δ-secretase transcription factor C/EBPβ (31) was highly augmented when the BDNF/TrkB pathway was eliminated (Fig. 3*C*, ninth and tenth panels from the top). Again, δ-secretase enzymatic activities were elevated in primary neurons depleting TrkB receptors (Fig. 3*D*). Immunofluorescent costaining further validated that KO of TrkB receptors elicited robust Tau N368 associated with extensive neuronal apoptosis (Fig. 3*E*), suggesting that BDNF/TrkB signaling reduction inhibits Akt and incurs δ-secretase activation and Tau N368 cleavage and neuronal loss. To further examine the role of BDNF/TrkB pathway-triggered Akt in mediating δ-secretase activation in vivo, we injected BDNF into the ventricular zone of mouse brains and tested p-TrkB/p-Akt/p-δ-secretase T322 pathways in the brains. We found that BDNF temporally activated p-TrkB and p-Akt in the hippocampus. Consistently, p-AEP T322 tightly coupled to p-Akt patterns and inversely correlated with δ-secretase cleavage (Fig. 3*F*), underscoring that p-δ-secretase T322 by Akt suppresses δ-secretase maturation and activation. Consequently, APP N585 and Tau N368 truncation closely fitted with δ-secretase activation. On the contrary, C/EBPβ and its active form p-C/EBPβ were decreased by BDNF administration, in alignment with δ-secretase expression reduction in the brain by BDNF (Fig. 3*F*, sixth panel from the top). Hence,

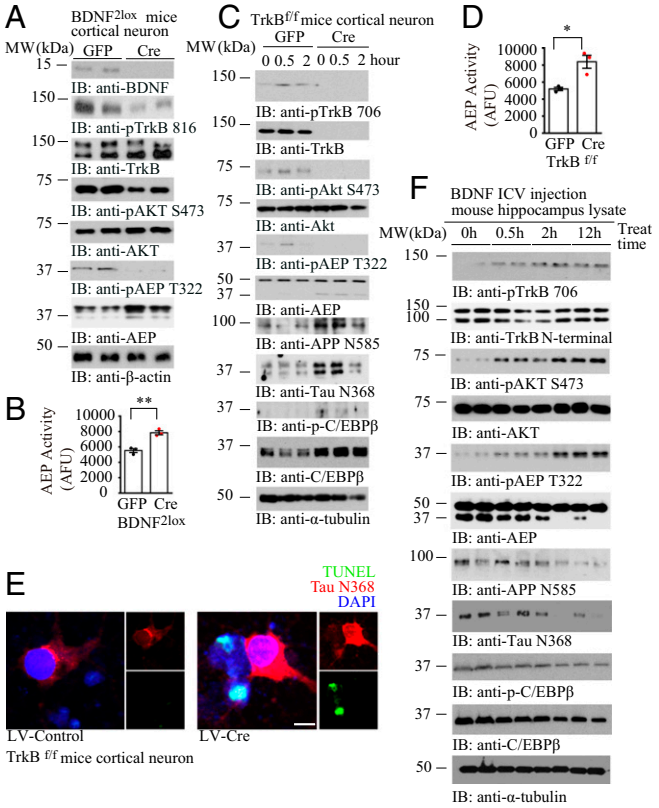

Fig. 3. BDNF/TrkB neurotrophic pathway mediates δ-secretase activity via T322 phosphorylation by Akt. (*A*) BDNF depletion inhibits p-Akt and p-AEP T322. $BDNF^{2lox}$ primary neuron was infected with Cre or GFP virus. Immunoblotting was conducted with neuronal lysates with various indicated antibodies. (*B*) AEP enzymatic activity was escalated in primary neurons without BDNF. (Data represent mean ± SEM of three independent experiments; $^{**}P < 0.01$, two-tailed Student's *t* test.) (*C*) TrkB receptor elimination decreased p-Akt and p-AEP T322, eliciting AEP activation. TrkB f/f primary neuron was cultured with AAV-Cre or AAV-GFP virus infection, followed by BDNF (50 ng/mL) for the indicated time points. Immunoblotting was performed with various indicated antibodies. (*D*) TrkB receptor depletion induces AEP enzymatic activity elevation. (Data represent mean ± SEM of three independent experiments; $^{*}P < 0.05$, two-tailed Student's *t* test.) (*E*) TrkB depletion incurs Tau N368 and neuronal apoptosis in primary neurons. Primary TrkB f/f neurons were infected with lentivirus expressing control or Cre, and immunofluorescent costaining was conducted. (Scale bar, 10 μm.) (*F*) BDNF intracerebroventricular (ICV) injection activates p-TrkB/p-Akt pathways, suppressing AEP activation. WT mice (8 mo old) were injected with BDNF (0.2 μg) into the ventricular zone and killed at the indicated time points. Hippocampal lysates were analyzed by immunoblotting with various antibodies.

BDNF/TrkB neurotrophic pathway dictates δ-secretase activation via Akt-mediated p-T322. BDNF or TrkB depletion elicits δ-secretase activation by inhibiting Akt.

BDNF Depletion-Triggered Tau N368 Cleavage and Synaptic Dysfunction in BDNF^{2lox} Mice Rescued by the Blocking Peptide. To examine whether depletion of BDNF in vivo also elicits Tau N368 production, leading to its association with and inhibition of TrkB signaling, we employed BDNF^{2lox} mice with viral vector-mediated expression of Cre in the hippocampus. One week following the viral injection, we incubated the brain lysates in the presence of FITC-conjugated TAT-R1 peptide from Tau R1 or TAT-control sR1 peptide, followed by immunoprecipitation with anti-Tau N368. Notably, the BDNF depletion-triggered Tau N368/TrkB complex was reduced by R1 compared with sR1 (*SI Appendix*, Fig. S3*A*). After treating the mice with FITC-conjugated TAT-R1 peptide from R1 or TAT-control peptide via i.p. administration (10 mg/kg) once every 5 d for 6 wk, we found that the i.p.-administered peptides were brain-permeable as validated by fluorescence examination of the brain sections. The peptides were demonstrable in the brain even 7 d after i.p. administration (*SI Appendix*, Fig. S3*B*), indicating that they could reach the target cell types with a long $t_{1/2}$ and detectable brain exposure. Co-IP with hippocampal tissues revealed that BDNF depletion induced an association between Tau N368 and TrkB in control peptide-treated samples. By contrast, the interaction was substantially diminished by treatment with R1 peptide (Fig. 4*A*). Accordingly, immunoblotting analysis showed that R1 treatment restored p-TrkB/p-Akt/p-MAPK signaling pathways, leading to repression of δ-secretase activation, Tau N368 truncation, and inhibition of caspase-3 activation compared with treatment with the control peptide (Fig. 4*B*). Interestingly, a minuscule amount of BDNF was demonstrable in R1-treated samples as opposed to the complete absence of BDNF in the control peptide group, suggesting that the cells protected by R1 peptide might produce some BDNF. Hence, BDNF depletion-triggered δ-secretase activation and subsequent Tau N368/TrkB association is selectively blocked by R1 peptide but not the control peptide, suggesting that Tau N368 binding to TrkB might be responsible for the adverse events.

BDNF/TrkB plays an essential role in synaptogenesis, synaptic plasticity, and learning and memory. Therefore, we performed EM analysis to examine the synapses in the hippocampus of BDNF$^{2lox/Cre}$ mice treated with these peptides. The synaptic density in the hippocampi of R1 peptide-treated mice was significantly higher than that seen in animals treated with the control peptide (*SI Appendix*, Fig. S3*C*). Immunohistochemistry staining showed that BDNF was depleted under both conditions (*SI Appendix*, Fig. S3*D*). NeuN staining demonstrated that R1 treatment substantially prevented neuronal loss induced by BDNF depletion compared with sR1 peptide treatment (*SI Appendix*, Fig. S3*E*). Consistent with immunoblotting analysis, immunofluorescent costaining showed that R1 decreased Tau N368 levels and escalated p-TrkB Y816 in the hippocampus, and the inverse correlation between Tau N368 and p-TrkB Y816 occurred with sR1 treatment (*SI Appendix*, Fig. S3*F*). Golgi staining also supported that dendritic spine density was also increased by R1 vs. control (Fig. 4*C*). Electrophysiological analysis found that the paired-pulse ratios (PPRs) were decreased in the control peptide group, when BDNF was depleted, and this impairment was significantly alleviated by R1 treatment (Fig. 4*D*). Next, we assessed the effect of dissociation of Tau N368 from TrkB in BDNF$^{2lox/Cre}$ mice by R1 peptide on memory functions in a Morris water maze (MWM). During the training phase, the swim distance and latency to find the platform were gradually decreased, demonstrating a learning effect in these BDNF-depleted mice, but both groups behaved similarly regardless of R1 or control peptide treatment. However, a probe trail found that R1 treatment increased memory retention in BDNF-KO mice, as illustrated by the higher percentage of time spent in the target quadrant. All groups of mice displayed

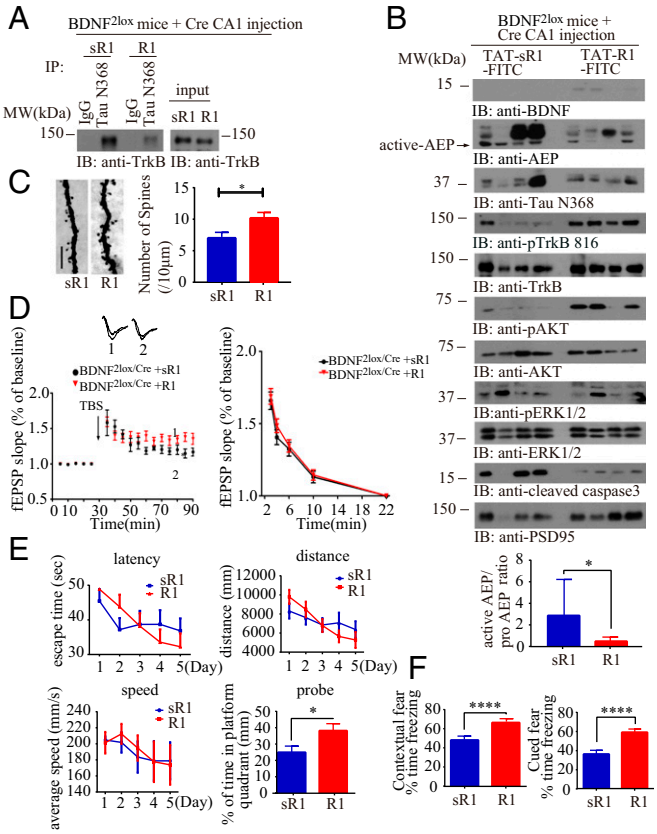

Fig. 4. BDNF depletion-triggered Tau N368 cleavage and synaptic dysfunctions are rescued by Tau R1 blocking peptide. (*A*) BDNF KO induces the interaction between Tau N368 and TrkB, which can be blocked by Tau R1 peptide. BDNF^{2lox} mice were injected with AAV-Cre virus and treated 1 wk later with FITC-conjugated TAT-R1 peptide. Brain lysates were immunoprecipitated with anti-Tau N368 and coprecipitated by anti-TrkB. (*B*) R1 peptide treatment restores p-TrkB signaling and inhibits AEP and caspase-3 activation. Brain lysates were analyzed with various indicated antibodies (*Top*). Tau R1 repressed AEP activity. (*Bottom*) Bar graph shows AEP activity quantification as mean ± SEM ($n = 3$ independent experiments; $^*P < 0.05$). (*C*) Golgi staining was conducted on brain sections from CA1 regions of mice (mean ± SEM; $n = 4$ mice per group; $^*P < 0.05$). (Scale bar, 5 μm.) (*D*) Electrophysiology analysis. R1 treatment rescued LTP defects in BDNF f/f AAV-Cre–injected mice (*Left*). (Mean ± SEM; $n = 6$ mice per group; $^*P < 0.05$.) (*E* and *F*) Tau R1 peptide treatment recovers cognitive functions in BDNF-depleted mice: MWM (*E*) and fear conditioning tests (*F*). (Mean ± SEM; $n = 9$ mice per group; $^*P < 0.05$, $^{****}P < 0.001$.)

comparable swim speeds, suggesting that depletion of BDNF did not have any detrimental effect on motor functions (Fig. 4*E*). Moreover, we conducted contextual and cued fear conditioning tests with these animals. R1 treatment significantly increased the memory in both tests compared with control peptide (Fig. 4*F*). Therefore, R1 peptide treatment disrupts BDNF depletion-triggered Tau N368 association with TrkB, up-regulating neurotrophic signaling, synaptic plasticity, and learning and memory in BDNF$^{2lox/Cre}$ mice.

KO of BDNF Induces AD-Like Pathology That Can Be Rescued by AEP-Uncleavable Tau N255A/N368A. To assess whether BDNF eradication-elicited TrkB signaling reduction and neuronal cell death are indeed mediated by δ-secretase–cleaved Tau N368 in vivo, we injected the Cre virus into the hippocampus of BDNF^{2lox} mice together with a vector expressing the δ-secretase–uncleavable form of Tau (N255A/N368A). As a control for CRE, we also injected the hippocampus with a GFP vector. As expected, the Cre virus completely abolished BDNF in the Cre group, whereas weak BDNF expression

was detectable in the Cre + Tau N255A/N368A group (Fig. 5*A*, *Top*). The corresponding IHC staining showed that BDNF was removed by Cre virus in the hippocampus of BDNF^{2lox} mice (Fig. 5*B*, *Top*). As expected, δ-secretase was strongly activated when BDNF was entirely depleted. By contrast, levels of its mature and active form were lower in the GFP or Cre + Tau N255A/N368A groups. Consistently, the Tau N368 fragment corresponded to the levels of active AEP (Fig. 5*A*, second and fourth panels). Consequently, p-TrkB/p-Akt/p-MAPK was blunted in the Cre + control group, whereas the phosphorylation remained intact in GFP or Cre + Tau N255A/N368A groups. Consequently, caspase-3 was activated when BDNF was completely eliminated, but its activation was barely detectable in the GFP control or Cre + Tau N255A/N368A groups (Fig. 5*A*, fourth panel from the bottom). These observations suggest that δ-secretase–cleaved Tau is indispensable for BDNF depletion-elicited neurotrophic activity suppression and neuronal apoptosis. Co-IP with the hippocampal lysates revealed that BDNF depletion provoked an association between Tau N368 and TrkB in the Cre + control group, but this complex was not detectable in GFP control or Cre + uncleavable Tau mutant groups (*SI Appendix*, Fig. S4*A*). Tau N368 staining corresponded to the immunoblotting results, and depletion of BDNF induced robust Tau N368 production in the Cre + control group (Fig. 5*B*, second panel from top). NeuN staining and quantitative neuronal counting analysis demonstrated that removal of BDNF elicited substantial hippocampal neurodegeneration compared with GFP control, but, in the presence of uncleavable Tau N255A/N368A, the neuronal loss was abrogated (Fig. 5*B*, third panel from top). Immunofluorescent staining showed that eradication of BDNF with Cre virus abolished

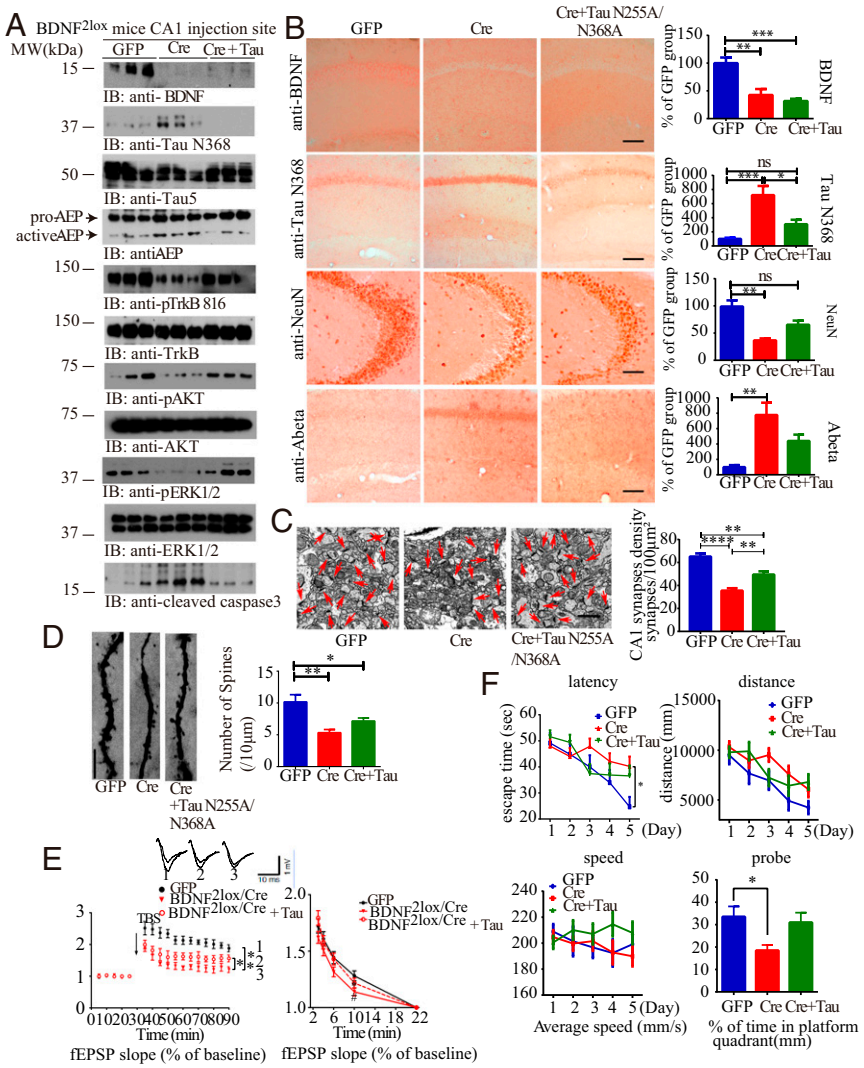

Fig. 5. Tau N368 cleavage by δ-secretase is required for BDNF KO-induced AD-like pathology. (*A*) Tau cleavage by AEP mediates BDNF depletion-induced AEP activation and TrkB signaling inhibition. BDNF^{2lox} mice were injected with AAV-GFP control, AAV-Cre virus, or AAV-Cre virus + uncleavable Tau N255A/N368A mutant virus in the CA1 region for 3 mo. Injection-site tissues were analyzed by immunoblotting with various antibodies (n = 3 mice per group). (*B*) Uncleavable Tau mutant decreases BDNF depletion-induced Tau N368 production and neuronal loss. IHC staining and quantitative analysis are shown (mean ± SEM; n = 12–16 sections from three mice in each group; *P < 0.05, **P < 0.01, and ***P < 0.001, one-way ANOVA). (Scale bar, 50 μm.) (*C*) EM of synapses (arrows; *Left*). (Scale bar, 1 μm.) Quantification of synaptic density (*Right*; mean ± SEM; n = 6 mice per group; **P < 0.01 and ****P < 0.0001, one-way ANOVA). (*D*) Golgi staining was conducted on brain sections from CA1 regions of mice (mean ± SEM; n = 4 mice per group; *P < 0.05 and ***P < 0.001, one-way ANOVA). (Scale bar, 5 μm.) (*E*) Electrophysiology analysis. (Mean ± SEM; n = 6 mice per group; *Left*, *P < 0.05 and **P < 0.01; *Right*, *P < 0.05, BDNF$^{2lox/cre}$ mice vs. BDNF$^{2lox/GFP}$ mice, $^{\#}P$ < 0.05, BDNF$^{2lox/cre}$ + Tau N255A/N368A mice vs. BDNF$^{2lox/cre}$ mice, one-way ANOVA.) Traces are representative fEPSPs recorded before and 60 min after theta-burst stimulation. (*F*) Analysis of MWM (mean ± SEM; n = 9 mice per group; *P < 0.05, one-way ANOVA).

p-TrkB Y816 in hippocampal neurons compared with GFP-treated controls, but expression of the uncleavable Tau mutant reversed the TrkB Y816 phosphorylation reduction caused by BDNF removal. Concordantly, apoptotic TUNEL staining was inversely related to TrkB phosphorylation (*SI Appendix*, Fig. S4*B*). As BDNF withdrawal also induces Aβ production (28), we also monitored Aβ IHC activity with anti-Aβ (6E10). Aβ levels were enhanced in the Cre + control group, whereas it was barely detectable in GFP or Cre + Tau N255A/N368A groups (Fig. 5*B*, fourth panel from top).

EM analysis revealed prominent synapses reduction in BDNF-KO samples compared with GFP-treated controls. However, the synaptic density of the hippocampus was significantly increased in the presence of the uncleavable form of Tau (N255A/N368A; Fig. 5*C*). Golgi staining showed that the dendritic spine density also exhibited the same pattern (Fig. 5*D*). Hence, BDNF KO in the hippocampus caused a reduction in synapses and dendritic spines, which was alleviated by preventing Tau cleavage by δ-secretase. Fitting with this observation, an electrophysiological analysis showed that the PPR was decreased when BDNF was removed compared with GFP control. LTP is a measure of synaptic plasticity that underlies learning and memory. The LTP amplitudes in $BDNF^{2lox/Cre}$ mice were ameliorated by Tau N255A/N368A. The electrophysiological defects triggered by BDNF removal were lessened by uncleavable Tau mutant (Fig. 5*E*). Taken together, these results indicate that BDNF deprivation-induced δ-secretase cleavage of Tau attributes to synaptic dysfunction. Cognitive behavioral tests in MWM showed that the latency for GFP and Cre + Tau mutant groups was significantly decreased vs. the Cre + control group. Correspondingly, in the probe trial, BDNF-KO mice (Cre + control) spent much less time in the target quadrant where the platform was submerged vs. the GFP control group. Coinfection of uncleavable Tau mutant rescued these memory deficits (Fig. 5*F*). We made the same observation with the cue fear conditioning and contextual fear conditioning (*SI Appendix*, Fig. S4*C*). As expected, inflammatory cytokines including TNF-α and IL-1β were significantly elevated when BDNF was depleted compared with GFP control and Cre + uncleavable Tau mutant groups (*SI Appendix*, Fig. S4*D*). Interestingly, Aβ42 but not Aβ40 concentrations were increased in hippocampal tissues when BDNF was knocked out; by contrast, expression of the uncleavable Tau mutant significantly repressed this effect (*SI Appendix*, Fig. S4*E*).

To further explore the molecular events in depth, we prepared primary neuronal cultures from $BDNF^{2lox}$ mice and infected the neurons with various vectors expressing GFP or Cre or Cre + uncleavable Tau mutant. Immunoblotting showed that BDNF was clearly deleted by Cre expression. Noticeably, Tau N368 levels were enhanced when BDNF was eliminated, whereas its level was ablated in the cells expressing the uncleavable Tau mutant, which was validated by HT7 antibody. Consistent with these findings, δ-secretase was activated in the absence of BDNF, and this activation was reduced in cells expressing the uncleavable Tau mutant (*SI Appendix*, Fig. S4*F*, *Left*, from top to bottom). The neurotrophic signaling cascade of p-TrkB/p-Akt/p-MAPK was attenuated when BDNF was knocked out by Cre virus compared with GFP control, but the neurotrophic signaling was partially rescued in the presence of the uncleavable Tau mutant (*SI Appendix*, Fig. S4*F*, *Right*). LDH assay with neuronal medium indicated that neuronal apoptosis was induced by BDNF removal compared with control, and apoptosis was significantly lower with expression of Tau N255A/N368A mutant (*SI Appendix*, Fig. S4*G*). Hence, Tau proteolytic cleavage by δ-secretase and subsequent inhibition of TrkB receptors via direct binding is indispensable for mediating the pathological effects upon BDNF depletion in the brain.

Discussion

In the present study, we found that Tau, especially the δ-secretase–truncated Tau N368 fragment, specifically binds to TrkB receptors, an interaction that is antagonized by BDNF. Tau N368 strongly interacts with the TrkB receptor C-terminal tail, a site of PLC-γ1 binding. This action is down-regulated by the presence of BDNF. Mapping assay further demonstrates that the R1 region in Tau is implicated in binding to the TrkB. Accordingly, TAT-conjugated R1 peptide dissociates BDNF depletion-triggered Tau N368/TrkB complex in the brain after i.p. administration in $BDNF^{2lox}$ mice, restoring TrkB neurotrophic signaling and inhibiting neuronal apoptosis. Interestingly, we found that BDNF deprivation with anti-BDNF or gene KO in primary neurons elicits δ-secretase activation and the resultant cleavage of Tau, yielding Tau N368 fragment. Although δ-secretase cleaves Tau at N255 and N368 residues, N368 is much more prominently cleaved by δ-secretase, so we mainly focused on this specific site. Here we show that BDNF/TrkB-activated Akt phosphorylates δ-secretase T322 and inhibits its activation; thus, depletion of BDNF inhibits Akt activity and triggers AEP activation by repressing T322 phosphorylation by Akt. Mammalian δ-secretase is a lysosomal cysteine protease that specifically cleaves after asparagine residues. δ-Secretase activation is autocatalytic; it requires sequential removal of C- and N-terminal propeptides at different pH thresholds. A previous study demonstrated that activation of the 56-kDa δ-secretase requires caspase-3 to cleave residue D25 in the N terminus of δ-secretase to generate the 36-kDa mature active form (17). Conceivably, BDNF withdrawal-activated caspase-3 may also contribute to δ-secretase activation. It is also possible that δ-secretase is posttranslationally modified in a fashion that might regulate δ-secretase activation as well. For instance, recently, we reported that SRPK2 phosphorylates δ-secretase on S226 in AD, mediating its cytoplasmic translocation and activation (22). To clarify the role of δ-secretase in mediating BDNF deprivation-induced neuronal cell death, we employed δ-secretase–null primary neurons (*SI Appendix*, Fig. S2 *C* and *D*). We found that anti-BDNF substantially diminishes its proapoptotic actions in $\delta\text{-secretase}^{-/-}$ neurons. Caspase-3 activation in the neurons was decreased as well. Hence, these data strongly support that δ-secretase activation is required for BDNF deprivation-induced neuronal cell death.

BDNF binds to TrkB receptors and triggers dimerization and autophosphorylation on numerous tyrosine residues on the intracellular domain. Phosphorylation and recruitment of adaptors to p-Y515 on TrkB leads to activation of the Ras/Raf/MAPK signaling cascade, which promotes neuronal differentiation and growth through MEK and MAPK and activation of the PI3K/Akt cascade, which promotes survival and growth of neurons and other cells through Ras or GRB-associated binder 1 (GAB1) (32). Recruitment and activation of PLC-γ1 through phosphorylation of p-Y816 results in the generation of inositol-1,4,5-trisphosphate and diacylglycerol, which is essential for BDNF-mediated synaptic plasticity (2, 33). Interestingly, we found that the Tau N368 fragment dose-dependently blocks TrkB signaling, enhancing caspase-3 activation (Fig. 2*D*). A mapping assay demonstrated that Tau interacts with TrkB C-terminal tail via the R1 domain, where PLC-γ1 binds (*SI Appendix*, Fig. S1). Thus, it is possible that Tau N368 associates with the C-terminal tail of TrkB and blocks p-Y816 phosphorylation, inhibiting PLC-γ1 activation and repressing synaptic plasticity. It remains unclear why binding to the tail domain on the TrkB receptor by Tau N368 affects both p-Akt and p-MAPK activation. Conceivably, Tau interaction with TrkB receptors might prevent the receptor tyrosine kinase autophosphorylation and subsequent activation. As PI3K/Akt plays such an important role in promoting cell survival and Tau N368 strongly antagonizes this prosurvival pathway, conceivably, Tau N368 exerts its neurotoxicity at least partially via suppressing PI3K/Akt pathway, inducing neuronal apoptosis.

Mounting evidence suggests that BDNF/TrkB signaling is an important regulator of amyloidogenic processing. For example, Aβ production in cultured cells is reduced by BDNF treatment (34), whereas it is facilitated by BDNF deprivation (28). On the

contrary, Aβ protein can directly inhibit the proteolytic conversion of BDNF from pro-BDNF, thus reducing its levels (35). In addition, Aβ indirectly affects BDNF levels at the synapse by interfering with its axonal transport. Aβ also inhibits retrograde axonal transport of the BDNF–TrkB complex (36). There is also direct evidence that administration of oligomeric Aβ significantly down-regulates BDNF expression in vitro (37, 38). Moreover, aggregated Aβ down-regulates the specific BDNF transcripts in AD (6). However, genetic knockdown of BDNF in 3xTg-AD (3xTg/BDNF$^{+/-}$) mice does not alter Aβ or Tau pathology because chronic reduction of BDNF does not exacerbate the development of Aβ and Tau pathology (39). Nevertheless, TrkB reduction aggravates AD-like signaling aberrations and memory deficits without affecting β-amyloidosis in 5XFAD mice (TrkB$^{+/-}$/5XFAD) (40). In these studies, although BDNF or TrkB is partially eliminated, neurotrophic signaling remains intact, which may explain the failure to observe alteration of Aβ or Tau pathologies. Nevertheless, in these AD mouse models, the high baseline Aβ and Tau levels might block the pathological effects induced by BDNF depletion. Unlike in our findings, BDNF withdrawal inhibits AEP T322 phosphorylation by Akt and elicits its robust activation that subsequently cuts Tau at N368, which, in turn, inhibits TrkB neurotrophic signaling pathways, further amplifying the antagonistic effect of Tau pathology on BDNF signaling. These observations implicate Tau pathology in neurotrophin dysregulation, which may represent a mechanism through which Tau confers toxicity in AD and related non-Alzheimer's dementias. Together, our data strongly suggest that Tau N368 exerts its neurotoxicity in AD directly through binding to TrkB receptors and blocking its neurotrophic signaling, triggering apoptotic caspase-3 activation, and this deleterious effect is δ-secretase–dependent. Clearance of Tau N368 via its specific antibody may exhibit promising therapeutic efficacy in AD mouse models. Because δ-secretase and Tau N368 are highly elevated in AD patient brains, our finding supports that inhibition of δ-secretase or Tau N368 via immunotherapy may be a novel potential strategy in the treatment of AD.

ACKNOWLEDGMENTS. We thank the Alzheimer's Disease Research Center at Emory University for human AD patients and healthy control samples. This work was supported by National Institute on Aging/National Institutes of Health Grant RFO1 AG051538 (to K.Y.).

1. Huang EJ, Reichardt LF (2001) Neurotrophins: Roles in neuronal development and function. *Annu Rev Neurosci* 24:677–736.
2. Minichiello L (2009) TrkB signalling pathways in LTP and learning. *Nat Rev Neurosci* 10:850–860.
3. Ferrer I, et al. (1999) BDNF and full-length and truncated TrkB expression in Alzheimer disease. Implications in therapeutic strategies. *J Neuropathol Exp Neurol* 58:729–739.
4. Garzon D, Yu G, Fahnestock M (2002) A new brain-derived neurotrophic factor transcript and decrease in brain-derived neurotrophic factor transcripts 1, 2 and 3 in Alzheimer's disease parietal cortex. *J Neurochem* 82:1058–1064.
5. Ginsberg SD, Che S, Wuu J, Counts SE, Mufson EJ (2006) Down regulation of trk but not p75NTR gene expression in single cholinergic basal forebrain neurons mark the progression of Alzheimer's disease. *J Neurochem* 97:475–487.
6. Peng S, et al. (2009) Decreased brain-derived neurotrophic factor depends on amyloid aggregation state in transgenic mouse models of Alzheimer's disease. *J Neurosci* 29: 9321–9329.
7. Belrose JC, Masoudi R, Michalski B, Fahnestock M (2014) Increased pro-nerve growth factor and decreased brain-derived neurotrophic factor in non-Alzheimer's disease tauopathies. *Neurobiol Aging* 35:926–933.
8. Zuccato C, Cattaneo E (2009) Brain-derived neurotrophic factor in neurodegenerative diseases. *Nat Rev Neurol* 5:311–322.
9. Murer MG, et al. (1999) An immunohistochemical study of the distribution of brain-derived neurotrophic factor in the adult human brain, with particular reference to Alzheimer's disease. *Neuroscience* 88:1015–1032.
10. Arancibia S, et al. (2008) Protective effect of BDNF against beta-amyloid induced neurotoxicity in vitro and in vivo in rats. *Neurobiol Dis* 31:316–326.
11. Kitiyanant N, Kitiyanant Y, Svendsen CN, Thangnipon W (2012) BDNF-, IGF-1- and GDNF-secreting human neural progenitor cells rescue amyloid β-induced toxicity in cultured rat septal neurons. *Neurochem Res* 37:143–152.
12. Zeng Y, Zhao D, Xie CW (2010) Neurotrophins enhance CaMKII activity and rescue amyloid-β-induced deficits in hippocampal synaptic plasticity. *J Alzheimers Dis* 21: 823–831.
13. Criscuolo C, Fabiani C, Bonadonna C, Origlia N, Domenici L (2015) BDNF prevents amyloid-dependent impairment of LTP in the entorhinal cortex by attenuating p38 MAPK phosphorylation. *Neurobiol Aging* 36:1303–1309.
14. Mazzaro N, et al. (2016) Tau-driven neuronal and neurotrophic dysfunction in a mouse model of early tauopathy. *J Neurosci* 36:2086–2100.
15. Ando S, et al. (2002) Animal model of dementia induced by entorhinal synaptic damage and partial restoration of cognitive deficits by BDNF and carnitine. *J Neurosci Res* 70:519–527.
16. Zhang Z, et al. (2014) Cleavage of tau by asparagine endopeptidase mediates the neurofibrillary pathology in Alzheimer's disease. *Nat Med* 20:1254–1262.
17. Li DN, Matthews SP, Antoniou AN, Mazzeo D, Watts C (2003) Multistep autoactivation of asparaginyl endopeptidase in vitro and in vivo. *J Biol Chem* 278:38980–38990.
18. Liu Z, et al. (2008) Neuroprotective actions of PIKE-L by inhibition of SET proteolytic degradation by asparagine endopeptidase. *Mol Cell* 29:665–678.
19. Zhang Z, et al. (2015) Delta-secretase cleaves amyloid precursor protein and regulates the pathogenesis in Alzheimer's disease. *Nat Commun* 6:8762.
20. Zhang Z, et al. (2017) Inhibition of delta-secretase improves cognitive functions in mouse models of Alzheimer's disease. *Nat Commun* 8:14740.
21. Zhang Z, et al. (2017) Asparagine endopeptidase cleaves α-synuclein and mediates pathologic activities in Parkinson's disease. *Nat Struct Mol Biol* 24:632–642.
22. Wang ZH, et al. (2017) Delta-secretase phosphorylation by SRPK2 enhances its enzymatic activity, provoking pathogenesis in Alzheimer's disease. *Mol Cell* 67:812–825.e5.
23. Wang ZH, et al. (2018) BDNF inhibits neurodegenerative disease-associated asparaginyl endopeptidase activity via phosphorylation by AKT. *JCI Insight* 3:99007.
24. Atasoy IL, et al. (2017) Both secreted and the cellular levels of BDNF attenuated due to tau hyperphosphorylation in primary cultures of cortical neurons. *J Chem Neuroanat* 80:19–26.
25. Rosa E, et al. (2016) Tau downregulates BDNF expression in animal and cellular models of Alzheimer's disease. *Neurobiol Aging* 48:135–142.
26. Coffey ET, Akerman KE, Courtney MJ (1997) Brain derived neurotrophic factor induces a rapid upregulation of synaptophysin and tau proteins via the neurotrophin receptor TrkB in rat cerebellar granule cells. *Neurosci Lett* 227:177–180.
27. Chen Q, et al. (2014) The cellular distribution and Ser262 phosphorylation of tau protein are regulated by BDNF in vitro. *PLoS One* 9:e91793.
28. Matrone C, Ciotti MT, Mercanti D, Marolda R, Calissano P (2008) NGF and BDNF signaling control amyloidogenic route and Abeta production in hippocampal neurons. *Proc Natl Acad Sci USA* 105:13139–13144.
29. Sabri M, et al. (2012) Mechanisms of microthrombi formation after experimental subarachnoid hemorrhage. *Neuroscience* 224:26–37.
30. Yuede CM, et al. (2009) Effects of voluntary and forced exercise on plaque deposition, hippocampal volume, and behavior in the Tg2576 mouse model of Alzheimer's disease. *Neurobiol Dis* 35:426–432.
31. Wang Z-H, et al. (2018) C/EBPβ regulates delta-secretase expression and mediates pathogenesis in mouse models of Alzheimer's disease. *Nat Commun* 9:1784.
32. Reichardt LF (2006) Neurotrophin-regulated signalling pathways. *Philos Trans R Soc Lond B Biol Sci* 361:1545–1564.
33. Minichiello L, et al. (2002) Mechanism of TrkB-mediated hippocampal long-term potentiation. *Neuron* 36:121–137.
34. Rohe M, et al. (2009) Brain-derived neurotrophic factor reduces amyloidogenic processing through control of SORLA gene expression. *J Neurosci* 29:15472–15478.
35. Zheng Z, Sabirzhanov B, Keifer J (2010) Oligomeric amyloid-beta inhibits the proteolytic conversion of brain-derived neurotrophic factor (BDNF), AMPA receptor trafficking, and classical conditioning. *J Biol Chem* 285:34708–34717.
36. Poon WW, et al. (2013) β-Amyloid (Aβ) oligomers impair brain-derived neurotrophic factor retrograde trafficking by down-regulating ubiquitin C-terminal hydrolase, UCH-L1. *J Biol Chem* 288:16937–16948.
37. Garzon DJ, Fahnestock M (2007) Oligomeric amyloid decreases basal levels of brain-derived neurotrophic factor (BDNF) mRNA via specific downregulation of BDNF transcripts IV and V in differentiated human neuroblastoma cells. *J Neurosci* 27:2628–2635.
38. Rosa E, Fahnestock M (2015) CREB expression mediates amyloid β-induced basal BDNF downregulation. *Neurobiol Aging* 36:2406–2413.
39. Castello NA, Green KN, LaFerla FM (2012) Genetic knockdown of brain-derived neurotrophic factor in 3xTg-AD mice does not alter Aβ or tau pathology. *PLoS One* 7:e39566.
40. Devi L, Ohno M (2015) TrkB reduction exacerbates Alzheimer's disease-like signaling aberrations and memory deficits without affecting β-amyloidosis in 5XFAD mice. *Transl Psychiatry* 5:e562.